JSST
Journal of Space Science and Technology

P-ISSN: 2008-4560
E-ISSN: 2423-4516

Journal of Space Science and Technology

Vol. 18, No. 4, pp.32-47, 2025
https://doi.org/10.22034/jsst.2025.1588
Journal Homepage: https://jsstpub.com

Original Research Paper

Layerwise Theory for Free Vibration and Panel Flutter Analysis of VSCL Plates Using IGA

Mehdi Dabouee [1], Vahid Khalafi [2], and Hamidreza Zarei [3]

Department of Aerospace Engineering, Shahid Sattari Aeronautical University of Science and Technology, Tehran, Iran

ARTICLE INFO

Article History:

Received 21 August 2025
Revised 06 October 2025
Accepted 07 October 2025
Available Online 14 October 2025

Keywords:

Free vibration
Panel flutter
Variable-stiffness composites
Isogeometric analysis
Layerwise theory

ABSTRACT

This research examines the free vibration and panel flutter of composite laminates with curvilinear fibers. It employs the isogeometric analysis (IGA) framework along with layerwise theory. The growing utilization of composite structures in the aerospace and mechanical industries has led to the increasing popularity of variable-stiffness composite laminate (VSCL). These laminates with curvilinear fibers are designed to achieve customized mechanical properties and improve design efficiency. To achieve greater accuracy than equivalent single-layer theories (ESL) and improved computational efficiency compared to 3D elasticity models, a layerwise theory based on Ferreira's formulation was adopted. This approach uses the kinematic assumptions of first-order shear deformation theory (FSDT) to define the displacement field within each layer. Subsequently, the governing equations for free vibration and panel flutter are obtained from the Hamilton principle, utilizing first-order piston theory to model aerodynamic pressure. The geometric domain is discretized using the isogeometric analysis method, in which the cubic NURBS basis functions used for the exact geometric modeling are simultaneously employed as the approximation functions in the finite element formulation. Numerical results are obtained by solving the eigenvalue problem. A parametric study was performed to investigate the impact of several factors, including layup configuration, thickness ratios, fiber curvature, and boundary conditions of the VSCL plates. The findings demonstrate strong alignment with previous research, confirming the proposed formulation's accuracy and effectiveness.

* Corresponding Author's E-mail: khalafi@ssau.ac.ir

How to Cite this Article:
M. Dabouee, V. Khalafi, and H. Zarei, "Layerwise theory for free vibration and panel flutter analysis of VSCL plates using IGA," *Journal of Space Science and Technology*, Vol. 18, No. 4, pp. 32-47, 2025, https://doi.org/10.22034/jsst.2025.1588.

1. INTRODUCTION

Composite plates are broadly used across various engineering disciplines, including aerospace, mechanical, turbomachinery, civil, and marine industries. They are essential for creating structures that are both efficient and cost-effective. Recent technological advancements have led to the development of a new category of composite materials that feature curvilinear fibers. Since the 1990s, variable-stiffness composite laminates (VSCLs) have garnered significant research interest [1]. This class of materials enables a tailored, point-wise variation of stiffness throughout a structure, which can lead to enhanced structural performance and greater design flexibility compared to their conventional constant-stiffness composite laminate (CSCL) counterparts of equivalent weight [2]. Therefore, the primary objective of this study is the analysis of the free vibration and aeroelastic behavior of such structures, employing more accurate theoretical models and computational methods.

The first study on the free vibration of VSCL laminates was conducted by Abdalla et al. [3] using Classical Plate Theory and the Finite Element Method. Akhavan and Ribeiro [4] developed a novel p-version finite element formulation based on TSDT to compute the natural frequencies and mode shapes of moderately thick rectangular plates with curvilinear fibers. Subsequently, Yazdani and Ribeiro [5] proposed a p-version finite element formulation, based on a layerwise plate theory, for the free vibration analysis of thick VSCL plates. Hachemi et al. [6] performed static and dynamic analyses of VSCL sandwich plates using a layerwise theory and the p-version finite element method to investigate their mechanical behavior. Moreira et al. [7] presented the free vibration of VSCL plates using Reddy's layerwise theory. They developed two distinct layerwise models, implemented as User Elements (UEL) in the Abaqus software, which utilized the FSDT theory for the UEL1 model and TSDT for the UEL3 model in each layer.

Isogeometric Analysis (IGA) is a powerful numerical method first proposed by Hughes [8]. The core principle of this approach is the use of NURBS as the basis functions to simultaneously represent the exact geometry and approximate the unknown solution field. Because the geometry is represented precisely, the geometric approximation errors inherent in conventional domain meshing are eliminated. Consequently, it is possible to achieve accurate results with much coarser discretizations, resulting in a significant reduction in computational costs. Shojaee et al. [9] employed an IGA framework based on Kirchhoff plate theory to analyze the free vibration and buckling of thin, symmetric composite laminates. Thai et al. [10] and Guo et al. [11] were among the first to utilize an IGA formulation combined with a layerwise theory, in which first-order shear deformation assumptions are applied to each layer. They used this framework to study the static, free vibration, and buckling of composite laminates and sandwich plates. They reported that this formulation is free from shear locking, eliminating the need for a shear correction factor. Liu and Jeffers [12] employed isogeometric analysis (IGA) in conjunction with layerwise theory to investigate the static response of laminated composites characterized by dissimilar interlayer properties. Their proposed configuration was a sandwich structure consisting of a functionally graded (FG) core and composite face sheets. Fazilati and Khalafi [13] investigated the free vibration of perforated, variable-stiffness composite plates using a multi-patch IGA approach. Hasim and Kefal [14] studied the static response of square and circular plates reinforced with curvilinear fibers by employing an Isogeometric Analysis (IGA) formulation based on an enhanced zigzag theory. In their later research [15,16], they extended their analysis to multilayer composite plates that incorporated piezoelectric layers as well as both straight and curvilinear fibers. The governing equations were derived using the principle of virtual work, coupled with Reddy's layerwise theory. An isogeometric finite element approach was then employed to study forced response, bending, and vibrational behavior of these smart composite plates.

Regarding the flutter analysis of variable-stiffness composite plates, Stodieck et al. [17] optimized curvilinear fiber composite laminates to enhance the aeroelastic performance of a two-dimensional wing. Their findings indicated that, compared to optimized straight-fiber laminates, the use of curvilinear fibers could increase the aeroelastic instability speed by up to 7% and reduce the maximum wing root load by as much as 52%. Employing isogeometric analysis, Khalafi and

Fazilati [18] performed the supersonic flutter of skewed variable-stiffness composite panels subjected to yawed flow. In a subsequent study [19], they introduced a robust computational framework using a genetic algorithm to optimize fiber paths for flutter suppression. Fazilati [20] also analyzed the supersonic flutter of these panels in the presence of delamination using the HSDT plate theory. The aeroelastic stability of VSCL laminates in the supersonic flow regime was also examined by Akhavan and Ribeiro [21]. Based on a third-order shear deformation theory (TSDT) and modeling the aerodynamic forces with first-order linear piston theory, they computed the dynamic (flutter) and static (divergence) instability boundaries using the p-version finite element method.

Rahmanian et al. [22] investigated the flutter and post-flutter behavior of skew VSCL plates using a nonlinear aeroelastic formulation based on GDQ method for spatial discretization and the Newmark method for time integration. Navardi et al. [23] used an isogeometric methodology to analyze the aeroelastic properties of VSCL laminates, including skewed quadrilateral and circular configurations. Their formulation was based on TSDT theory with aerodynamic loading assumed by first-order piston theory. They subsequently extended this framework to the analysis of cylindrical panels [24]. Based on the Zig-Zag Theory, Hao et al. [25] presented an analysis of the aero-thermo-elastic behavior of composite laminates with curvilinear fibers subjected to supersonic flow in coupled thermal and aerodynamic environments. More recently, a flutter analysis of three-phase hybrid composite (carbon nanotube/polymer/ fiber) quadrilateral VSCL plates was developed by Fazilati et al. [26] to predict the impacts of nanostructured additives on the aeroelastic stability of structures with complex geometries.

Moreira et al. conducted comprehensive research on the aeroelastic stability of variable-stiffness composite plates in supersonic flow, employing a layerwise theory framework using the standard finite element methods. In their first study [27], they demonstrated the advantages of the layerwise approach for analyzing buckling and flutter of such laminates, especially when compared to ESL models. They then developed their layerwise model to investigate the flutter behavior of sandwich panels featuring curvilinear fiber composite face sheets and a viscoelastic core [28]. Extending further, they incorporated thermal effects to examine the aero-thermo-elastic stability of these structures [29]. Ultimately, their research progressed to explore active flutter control for smart sandwich panels outfitted with piezoelectric actuators and sensors [30].

A review of the existing literature shows that while the isogeometric approach (IGA) combined with layerwise theory has been utilized for the free vibration analysis of variable-stiffness composite plates, a significant gap exists in its application to aeroelasticity. To the authors' knowledge, this specific high-fidelity approach has not yet been developed for the panel flutter analysis of these advanced composites. The core novelty of this work is the development of a unified layerwise-IGA framework to address this problem, representing a significant step forward in both modelling accuracy and computational performance. Employing the IGA approach demonstrates a substantial improvement in computational efficiency over recent layerwise finite element models, achieving converged results with significantly coarser discretization. Therefore, this study focuses on developing an isogeometric formulation based upon Ferreira's layerwise model to investigate the vibration characteristics and panel flutter of VSCL composite laminates subjected to yawed supersonic flow.

2. VARIABLE STIFFNESS LAMINATED COMPOSITE

Variable stiffness in composite materials can be engineered using various techniques. In this study, Variable-Stiffness Laminated Composites (VSCL) are defined as laminates made with fibers arranged in curvilinear paths. In these composites, the fiber orientation angle changes continuously along the length of the plate, resulting in a different fiber tangent at each point. Consequently, the plate stiffness becomes a function of spatial position, varying point-by-point across the domain. The degree of curvature of the fiber path in each layer along the longitudinal direction (x-axis) is governed by two control angles, designated as T_0 and T_1.

Figute 1 provides a schematic of a single VSCL ply subjected to a yawed flow relative to the x-axis, along with the parameters that govern its fiber curvature. The fiber path within the k^{th} ply of the

VSCL plate is also assumed to vary linearly along the longitudinal direction (x-axis) and is expressed as follows [31]:

$$\theta^k(x) = \frac{2(T_1^k - T_0^k)}{a}|x| + T_0^k \quad (1)$$

where Λ is the yaw angle of the supersonic airflow with respect to the x-axis. For the k^{th} ply, T_0^k denotes the fiber orientation angle at the plate's longitudinal centerline (x=0), and T_1^k is the fiber angle at the vertical edges (x=±a/2). The fiber path of a VSCL ply is conventionally described by the notation $< T_0^k | T_1^k >$. Consequently, the stacking sequence for an *N*-ply laminate is expressed as $\left[< T_0^1 | T_1^1 >, < T_0^2 | T_1^2 >, \cdots, < T_0^N | T_1^N >\right]$. In the specific case where $T_0^k = T_1^k = T^k$, the notation simplifies to $< T^k | T^k >$, which represents a ply with straight, parallel fibers, characteristic of a conventional constant-stiffness composite laminate (CSCL).

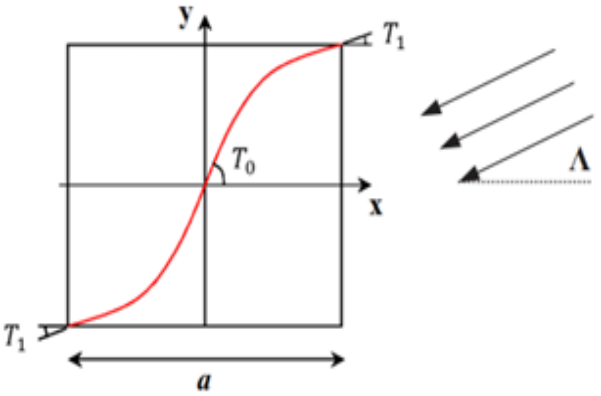

Fig 1. Control parameters defining the fiber path in a single VSCL ply subjected to a yawed flow.

3. ISOGEOMETRIC ANALYSIS

In the isogeometric analysis (IGA) method, B-spline and, more generally, Non-Uniform Rational B-Spline (NURBS) basis functions are employed as the shape functions. In this approach, the same NURBS basis functions that provide a precise geometric representation are simultaneously utilized to approximate the displacement field within the FE formulation. A B-spline represents a special case of a NURBS function where the weight associated with each control point is unity. A NURBS curve of order *p* is constructed using the following relation:

$$\mathbf{C}(\xi) = \sum_{i=1}^{n} R_{i,p}(\xi)\mathbf{P}_i = \sum_{i=1}^{n} \frac{N_{i,p}(\xi)\ w_i}{\sum_{j=1}^{n} N_{j,p}(\xi)\ w_j}\mathbf{P}_i \quad (2)$$

where $R_{i,p}$ is the NURBS basis function, $N_{i,p}$ is the B-spline function, and $\mathbf{P}_i$ and w_i are the spatial position and weight, respectively, of each control point defining the curve in the physical domain. The control points necessarily do not lie on the curve. The B-spline function, $N_{i,p}$, is defined by a recursive formula over a knot vector, $\Xi(\xi) = \{\xi_1 = 0, \cdots, \xi_i, \cdots, \xi_{n+p+1} = 1\}$, in the parametric space, where ξ_i are the knots. Each knot span, $[\xi_i \leq \xi_{i+1})$, is considered to be an element:

$$\begin{aligned} &for\ p = 0: \\ &N_{i,0}(\xi) = \begin{cases} 1 & if\ \xi_i \leq \xi < \xi_{i+1} \\ 0 & otherwise \end{cases} \\ &for\ p > 0: \\ &N_{i,p}(\xi) = \frac{\xi - \xi_i}{\xi_{i+p} - \xi_i} N_{i,p-1}(\xi) + \frac{\xi_{i+p+1} - \xi}{\xi_{i+p+1} - \xi_{i+1}} N_{i,p-1}(\xi) \end{aligned} \quad (3)$$

The expression for a NURBS surface is obtained by generalizing the basis functions of a NURBS curve along the x and y directions, as follows:

$$S(\xi,\eta) = \sum_{i=1}^{n}\sum_{j=1}^{m} R_{i,j}^{p,q}(\xi,\eta)\ \mathbf{P}_{i,j} = \sum_{i=1}^{n}\sum_{j=1}^{m} \frac{N_{i,p}(\xi)M_{j,q}(\eta)w_{i,j}}{W(\xi,\eta)}\mathbf{P}_{i,j} \quad (4)$$

and

$$W(\xi,\eta) = \sum_{i=1}^{n}\sum_{j=1}^{m} N_{i,p}(\xi)M_{j,q}(\eta)\ w_{i,j} \quad (5)$$

In the above relations, $R_{i,j}^{p,q}$ is the NURBS basis function; $N_{i,p}$ and $M_{j,q}$ are the B-spline basis functions of order *p* and *q* in the x- and y-directions, respectively. The terms $\mathbf{P}_{i,j}$ and $w_{i,j}$ denote the spatial coordinates vector and the associated weight of each point in the surface's $m \times n$ control net.

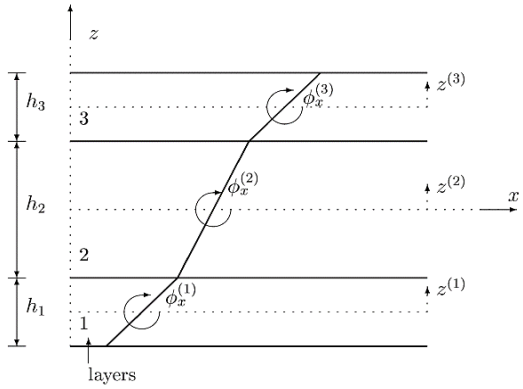

Fig. 2. Layerwise model kinematics for a three-layer laminate [10].

4. LAYERWISE DISPLACEMENT, STRAIN, AND STRESS FIELDS

This section presents the formulation of the layerwise theory, which is based on Ferreira's model [10] and incorporates FSD theory within each layer. The model is initially developed for a simple three-layer composite laminate, for which displacement continuity must be enforced at the interface where the top and bottom layers meet the middle layer. Subsequently, this formulation can easily be extended to laminates with multiple layers.

The displacement field of the top, middle, and bottom layers, identified by superscripts (1), (2), and (3), as illustrated in Fig. 2, are developed based upon the FSDT theory for each layer as follows [10]:

$$\begin{aligned} u^{(2)}(x,y,z) &= u_0 + z\,\psi_x^{(2)} \\ v^{(2)}(x,y,z) &= v_0 + z\,\psi_y^{(2)} \\ w^{(2)}(x,y,z) &= w_0 \end{aligned} \tag{6}$$

$$\begin{aligned} u^{(1)}(x,y,z) &= u_0 - \frac{h_1}{2}\psi_x^{(1)} - \frac{h_2}{2}\psi_x^{(2)} + z\,\psi_x^{(1)} \\ v^{(1)}(x,y,z) &= v_0 - \frac{h_1}{2}\psi_y^{(1)} - \frac{h_2}{2}\psi_y^{(2)} + z\,\psi_y^{(1)} \\ w^{(1)}(x,y,z) &= w_0 \end{aligned} \tag{7}$$

$$\begin{aligned} u^{(3)}(x,y,z) &= u_0 + \frac{h_2}{2}\psi_x^{(2)} + \frac{h_3}{2}\psi_x^{(3)} + z\,\psi_x^{(3)} \\ v^{(3)}(x,y,z) &= v_0 + \frac{h_2}{2}\psi_y^{(2)} + \frac{h_3}{2}\psi_y^{(3)} + z\,\psi_y^{(3)} \\ w^{(3)}(x,y,z) &= w_0 \end{aligned} \tag{8}$$

This formulation of the plate theory entails a total of nine degrees of freedom (DOFs) for the assumed displacement field. These comprise three displacements of the middle layer's mid-plane (u_0, v_0, w_0) and six rotational degrees of freedom ($\psi_x^{(1)}, \psi_y^{(1)}, \psi_x^{(2)}, \psi_y^{(2)}, \psi_x^{(3)}, \psi_y^{(3)}$) corresponding to the rotations of the transverse normal about the y- and x-axes for each respective layer. In Eqs. (6) through (8), h_k (where k=1,2,3) is the thickness of the k^{th} layer, and $z \in [-h_k/2,\ h_k/2]$ is the transverse coordinate measured from its corresponding mid-plane. The total thickness of the plate is denoted by h.

The corresponding strain components are derived from the displacement field using the following relations:

$$\left\{\boldsymbol{\varepsilon}_{in-p}^{(k)}\right\} = \begin{Bmatrix}\varepsilon_x \\ \varepsilon_y \\ \gamma_{xy}\end{Bmatrix}^{(m)} + \begin{Bmatrix}\varepsilon_x^{(k)} \\ \varepsilon_y^{(k)} \\ \gamma_{xy}^{(k)}\end{Bmatrix}^{(mb)} + z\begin{Bmatrix}\varepsilon_x^{(k)} \\ \varepsilon_y^{(k)} \\ \gamma_{xy}^{(k)}\end{Bmatrix}^{(b)} \tag{9}$$

Here, the superscripts m and b denote the membrane and bending components of the in-plane strain for the k^{th} layer, respectively, and mb indicates the coupling term. The membrane components are functions of the mid-plane deformation and are thus identical for all three layers. The bending components for each layer, however, are given by:

$$\begin{Bmatrix}\varepsilon_x \\ \varepsilon_y \\ \gamma_{xy}\end{Bmatrix}^{(m)} = \begin{Bmatrix} \dfrac{\partial u_0}{\partial x} \\ \dfrac{\partial v_0}{\partial y} \\ \dfrac{\partial u_0}{\partial y} + \dfrac{\partial v_0}{\partial x} \end{Bmatrix} \tag{10}$$

$$\begin{Bmatrix}\varepsilon_x^{(k)} \\ \varepsilon_y^{(k)} \\ \gamma_{xy}^{(k)}\end{Bmatrix}^{(b)} = \begin{Bmatrix} \dfrac{\partial \psi_x^{(k)}}{\partial x} \\ \dfrac{\partial \psi_y^{(k)}}{\partial y} \\ \dfrac{\partial \psi_x^{(k)}}{\partial y} + \dfrac{\partial \psi_y^{(k)}}{\partial x} \end{Bmatrix}, k = 1,2,3 \tag{11}$$

The coupling terms are introduced to satisfy the displacement continuity condition at the interlaminar interfaces. The membrane-bending strains for each layer are:

$$\begin{Bmatrix} \varepsilon_x^{(1)} \\ \varepsilon_y^{(1)} \\ \gamma_{xy}^{(1)} \end{Bmatrix}^{(mb)} = \begin{Bmatrix} -\frac{h_1}{2}\frac{\partial \psi_x^{(1)}}{\partial x} - \frac{h_2}{2}\frac{\partial \psi_x^{(2)}}{\partial x} \\ -\frac{h_1}{2}\frac{\partial \psi_y^{(1)}}{\partial y} - \frac{h_2}{2}\frac{\partial \psi_y^{(2)}}{\partial y} \\ -\frac{h_1}{2}\frac{\partial \psi_x^{(1)}}{\partial y} - \frac{h_2}{2}\frac{\partial \psi_x^{(2)}}{\partial y} - \frac{h_1}{2}\frac{\partial \psi_y^{(1)}}{\partial x} - \frac{h_2}{2}\frac{\partial \psi_y^{(2)}}{\partial x} \end{Bmatrix}$$

$$\begin{Bmatrix} \varepsilon_x^{(2)} \\ \varepsilon_y^{(2)} \\ \gamma_{xy}^{(2)} \end{Bmatrix}^{(mb)} = \begin{Bmatrix} 0 \\ 0 \\ 0 \end{Bmatrix} \tag{12}$$

$$\begin{Bmatrix} \varepsilon_x^{(3)} \\ \varepsilon_y^{(3)} \\ \gamma_{xy}^{(3)} \end{Bmatrix}^{(mb)} = \begin{Bmatrix} \frac{h_2}{2}\frac{\partial \psi_x^{(2)}}{\partial x} + \frac{h_3}{2}\frac{\partial \psi_x^{(3)}}{\partial x} \\ \frac{h_2}{2}\frac{\partial \psi_y^{(2)}}{\partial y} + \frac{h_3}{2}\frac{\partial \psi_y^{(3)}}{\partial y} \\ \frac{h_2}{2}\frac{\partial \psi_x^{(2)}}{\partial y} + \frac{h_3}{2}\frac{\partial \psi_x^{(3)}}{\partial y} + \frac{h_2}{2}\frac{\partial \psi_y^{(2)}}{\partial x} + \frac{h_3}{2}\frac{\partial \psi_y^{(3)}}{\partial x} \end{Bmatrix}$$

Similar to higher-order shear deformation theories (HSDTs), this model does not require a shear correction factor for the transverse shear strains, γ_{xz} and γ_{yz}. These strain components are defined as

$$\left\{\boldsymbol{\gamma}_{TS}^{(k)}\right\} = \begin{Bmatrix} \gamma_{yz}^{(k)} \\ \gamma_{xz}^{(k)} \end{Bmatrix} = \begin{Bmatrix} \frac{\partial w_0}{\partial y} + \psi_y^{(k)} \\ \frac{\partial w_0}{\partial x} + \psi_x^{(k)} \end{Bmatrix}, k = 1,2,3 \tag{13}$$

The constitutive equations for the k^{th} layer are formulated in the reference coordinate system based on Hooke's law. Applying the plane stress assumption, where the out-of-plane normal stress (σ_z) is considered negligible, these relations are given by:

$$\begin{Bmatrix} \sigma_x \\ \sigma_y \\ \tau_{xy} \\ \tau_{yz} \\ \tau_{xz} \end{Bmatrix}^{(k)} = \begin{bmatrix} \bar{Q}_{11} & \bar{Q}_{12} & \bar{Q}_{16} & 0 & 0 \\ \bar{Q}_{12} & \bar{Q}_{22} & \bar{Q}_{26} & 0 & 0 \\ \bar{Q}_{16} & \bar{Q}_{26} & \bar{Q}_{66} & 0 & 0 \\ 0 & 0 & 0 & \bar{Q}_{44} & \bar{Q}_{45} \\ 0 & 0 & 0 & \bar{Q}_{45} & \bar{Q}_{55} \end{bmatrix}^{(k)} \begin{Bmatrix} \varepsilon_x \\ \varepsilon_{yy} \\ \gamma_{xy} \\ \gamma_{xz} \\ \gamma_{yz} \end{Bmatrix}^{(k} \tag{14}$$

where $[\bar{Q}]^{(k)}$ is the transformed reduced stiffness matrix for the k^{th} layer, as defined in [32]. In a variable-stiffness lamina, as shown in Eq. (1), the fiber orientation angle θ is a function of the spatial coordinates. This makes the stiffness matrix $[\bar{Q}]^{(k)}$ inherently position-dependent, giving rise to the desired variable-stiffness behavior.

5. GOVERNING EQUATIONS

In this section, the weak form of the governing equation is derived through the application of Hamilton's principle. As this analysis considers only symmetric laminates, for which bending-stretching coupling is null, the in-plane displacement terms u_0 and v_0 are disregarded. This simplification reduces the degrees of freedom (DOF) per node from nine to seven, significantly decreasing the computational run time [10]. For unsymmetric laminates, a complete 9-DOF formulation would be required. The strain field for the symmetric case, therefore, simplifies to:

$$\left\{\boldsymbol{\varepsilon}_{in-p}^{(k)}\right\} = \begin{Bmatrix} \varepsilon_x^{(k)} \\ \varepsilon_y^{(k)} \\ \gamma_{xy}^{(k)} \end{Bmatrix} = \begin{Bmatrix} \varepsilon_x^{(k)} \\ \varepsilon_y^{(k)} \\ \gamma_{xy}^{(k)} \end{Bmatrix}^{(mb)} + z \begin{Bmatrix} \varepsilon_x^{(k)} \\ \varepsilon_y^{(k)} \\ \gamma_{xy}^{(k)} \end{Bmatrix}^{(b)} \tag{15}$$

Minimizing the total potential energy yields:

$$\delta\Pi = \int_0^t (\delta T + \delta U - \delta W_{ext})\, dt = 0 \tag{16}$$

where δT, δU, and δW_{ext} are the virtual kinetic energy, virtual strain energy, and the virtual work done by external forces, respectively. In the aeroelastic analysis, the pressure induced by the flow over the plate is considered the external work, and its effect must be incorporated into the governing equations. The resulting weak form for the three-layer system over the domain Ω is given by [23]:

$$\int_\Omega \left\langle \sum_{k=1}^{3} \left(\delta \left\{ \boldsymbol{\varepsilon}_{in-p}^{(k)} \right\}^T D_s^{(k)} \left\{ \varepsilon_{in-p}^{(k)} \right\} \right) + \sum_{k=1}^{3} \left(\delta \left\{ \boldsymbol{\gamma}_{TS}^{(k)} \right\}^T \mathrm{E}^{(k)} \left\{ \gamma_{TS}^{(k)} \right\} \right) \right\rangle d\Omega + \int_\Omega \Delta P\, \delta w_0\, d\Omega = \int_\Omega \left\langle \sum_{k=1}^{3} \left(\delta \left\{ u^{(k)} \right\}^T m \left\{ \ddot{u}^{(k)} \right\} \right) \right\rangle d\Omega \tag{17}$$

where

$$D_s^{(k)} = \begin{bmatrix} \mathrm{A}^{(k)} & \mathrm{B}^{(k)} \\ \mathrm{B}^{(k)} & \mathrm{D}^{(k)} \end{bmatrix}; \mathrm{E}^{(k)} = \begin{bmatrix} E_{44}^{(k)} & E_{45}^{(k)} \\ E_{45}^{(k)} & E_{55}^{(k)} \end{bmatrix} \quad (18)$$

$$\mathrm{m} = \begin{bmatrix} I_0^{(k)} & I_1^{(k)} \\ I_1^{(k)} & I_2^{(k)} \end{bmatrix}$$

and

$$\begin{aligned} &\left(\mathrm{A}_{ij}^{(k)}, B_{ij}^{(k)}, D_{ij}^{(k)}\right) \\ &= \int_{-h_k/2}^{h_k/2} \overline{\mathrm{Q}}_{ij}^{(k)}(1, z, z^2)\, dz \\ &, \quad (i,j = 1,2,6) \\ &E_{ij}^{(k)} = \int_{-h_k/2}^{h_k/2} \overline{\mathrm{Q}}_{ij}^{(k)}\, dz \quad , \quad (i,j = 4,5) \\ &\left(I_0^{(k)}, I_1^{(k)}, I_2^{(k)}\right) = \int_{-h_k/2}^{h_k/2} \rho\,(1, z, z^2)\, dz \end{aligned} \quad (19)$$

With $\hat{\boldsymbol{u}}^{(k)} = \left\{\mathbf{u}_1^{(k)} \quad \mathbf{u}_2^{(k)}\right\}^T$ and

$$\begin{Bmatrix} -\frac{h_1}{2}\psi_x^{(1)} - \frac{h_2}{2}\psi_x^{(2)} \\ -\frac{h_1}{2}\psi_y^{(1)} - \frac{h_2}{2}\psi_y^{(2)} \\ w_0 \end{Bmatrix}; \ \mathbf{u}_2^{(1)} = \begin{Bmatrix} \psi_x^{(1)} \\ \psi_y^{(1)} \\ 0 \end{Bmatrix};$$

$$\mathbf{u}_1^{(2)} = \begin{Bmatrix} 0 \\ 0 \\ w_0 \end{Bmatrix}; \mathbf{u}_2^{(2)} = \begin{Bmatrix} \psi_x^{(2)} \\ \psi_y^{(2)} \\ 0 \end{Bmatrix}; \quad (20)$$

$$\mathbf{u}_1^{(3)} = \begin{Bmatrix} \frac{h_2}{2}\psi_x^{(2)} + \frac{h_3}{2}\psi_x^{(3)} \\ \frac{h_2}{2}\psi_y^{(2)} + \frac{h_3}{2}\psi_y^{(3)} \\ w_0 \end{Bmatrix}; \mathbf{u}_2^{(3)} = \begin{Bmatrix} \psi_x^{(3)} \\ \psi_y^{(3)} \\ 0 \end{Bmatrix}$$

In the isogeometric approach, the displacement field (**u**) is approximated using the NURBS basis functions, R_I. Within the context of the presented layerwise theory, this leads to a seven-degree-of-freedom approximation for the displacement field as follows:

$$\begin{aligned} &\mathbf{u} \\ &= \left\{ w_0, \psi_x^{(1)}, \psi_y^{(1)}, \psi_x^{(2)}, \psi_y^{(2)}, \psi_x^{(3)}, \psi_y^{(3)} \right\}^T \\ &= \sum_{I=1}^{m\times n} \boldsymbol{R}_I\, \boldsymbol{q}_I \end{aligned} \quad (21)$$

where $\boldsymbol{q}_I^T = \left\{w_{0_I}, \psi_{xI}^{(1)}, \psi_{yI}^{(1)}, \psi_{xI}^{(2)}, \psi_{yI}^{(2)}, \psi_{xI}^{(3)}, \psi_{yI}^{(3)}\right\}$ is the vector of nodal degrees of freedom corresponding to the I[th] control point within the $m \times n$ control mesh. The term $\boldsymbol{R}_I$ represents the shape function matrix.

$$\mathbf{u} = \begin{bmatrix} R_I & 0 & 0 & 0 & 0 & 0 & 0 \\ 0 & R_I & 0 & 0 & 0 & 0 & 0 \\ 0 & 0 & R_I & 0 & 0 & 0 & 0 \\ 0 & 0 & 0 & R_I & 0 & 0 & 0 \\ 0 & 0 & 0 & 0 & R_I & 0 & 0 \\ 0 & 0 & 0 & 0 & 0 & R_I & 0 \\ 0 & 0 & 0 & 0 & 0 & 0 & R_I \end{bmatrix} \begin{Bmatrix} w_{0_I} \\ \psi_{xI}^{(1)} \\ \psi_{yI}^{(1)} \\ \psi_{xI}^{(2)} \\ \psi_{yI}^{(2)} \\ \psi_{xI}^{(3)} \\ \psi_{yI}^{(3)} \end{Bmatrix} \quad (22)$$

Substituting the vector of degrees of freedom into Eqs. (13) and (15) yields the following strain-displacement relationship [31]:

$$\begin{aligned} &\{\boldsymbol{\varepsilon}_{in-p} \quad \boldsymbol{\gamma}_{TS}\}^T = \sum_{I=1}^{m\times n} \mathbf{B}_I\, \boldsymbol{q}_I \\ &= \sum_{I=1}^{m\times n} \left[\begin{Bmatrix} \mathbf{B}_I^{mb(1)} \\ \mathbf{B}_I^{mb(2)} \\ \mathbf{B}_I^{mb(3)} \end{Bmatrix}^T \begin{Bmatrix} \mathbf{B}_I^{b(1)} \\ \mathbf{B}_I^{b(2)} \\ \mathbf{B}_I^{b(3)} \end{Bmatrix}^T \begin{Bmatrix} \mathbf{B}_I^{s(1)} \\ \mathbf{B}_I^{s(2)} \\ \mathbf{B}_I^{s(3)} \end{Bmatrix}^T \right]^T \boldsymbol{q}_I \end{aligned} \quad (23)$$

For the top layer (k=1):

$$\mathbf{B}_I^{mb(1)} = \begin{bmatrix} 0 & \frac{-h_1}{2}R_{I,x} & 0 & \frac{-h_2}{2}R_{I,x} & 0 & 0 & 0 \\ 0 & 0 & \frac{-h_1}{2}R_{I,y} & 0 & \frac{-h_2}{2}R_{I,y} & 0 & 0 \\ 0 & \frac{-h_1}{2}R_{I,y} & \frac{-h_1}{2}R_{I,x} & \frac{-h_2}{2}R_{I,y} & \frac{-h_2}{2}R_{I,x} & 0 & 0 \end{bmatrix}$$

$$\mathbf{B}_I^{b(1)} = \begin{bmatrix} 0 & R_{I,x} & 0 & 0 & 0 & 0 & 0 \\ 0 & 0 & R_{I,y} & 0 & 0 & 0 & 0 \\ 0 & R_{I,y} & R_{I,x} & 0 & 0 & 0 & 0 \end{bmatrix}; \quad (24)$$

$$\mathbf{B}_I^{s(1)} = \begin{bmatrix} R_{I,y} & 0 & R_I & 0 & 0 & 0 & 0 \\ R_{I,x} & R_I & 0 & 0 & 0 & 0 & 0 \end{bmatrix}$$

Similarly, the components of matrix **B** can be derived for the second and third layers.

The external work in Eq. (17) is performed by the aerodynamic pressure (ΔP). This pressure is modelled using the first-order piston theory, but its application is subject to certain limitations. The theory is valid within the Mach number range of $\sqrt{2} < M_\infty < 5$ to avoid singularities near the transonic regime and inaccuracies in the hypersonic regime. Furthermore, its foundation on small disturbance theory makes it suitable for predicting the linear onset of flutter, but not for non-linear post-flutter

analysis. As the objective of this work is to determine the critical flutter boundary, this theory is an appropriate choice. The expression for the pressure, accounting for the yaw angle (Λ), is given by [33]:

$$\Delta P = -\frac{\rho_\infty U_\infty^2}{\sqrt{M_\infty^2-1}}\left(\frac{\partial w}{\partial x}\cos\Lambda + \frac{\partial w}{\partial y}\sin\Lambda + \frac{1}{U_\infty}\left(\frac{M_\infty^2-2}{M_\infty^2-1}\right)\frac{\partial w}{\partial t}\right) \quad (25)$$

where ρ_∞, U_∞, and M_∞ are the flow density, velocity, and Mach number, respectively, and Λ is the flow yaw angle. The non-dimensional aerodynamic pressure is then defined as:

$$\lambda = \frac{\rho_\infty U_\infty^2 a^3}{\beta\, D_0} \quad (26)$$

in which the dimensionless parameters β and D_0 are given by:

$$\beta = \sqrt{M_\infty^2-1}\ ,\ D_0 = \frac{E_1 h^3}{12(1-\nu_{12}\nu_{21})} \quad (27)$$

In the supersonic regime ($M_\infty > 1$), the expression for the aerodynamic pressure takes the following form [18]:

$$\Delta P = \lambda\left(\frac{\partial w}{\partial x}\cos\Lambda + \frac{\partial w}{\partial y}\sin\Lambda\right) + \sqrt{\frac{\lambda\mu}{M_\infty}}\left(\frac{\partial w}{\partial t}\right) \quad (28)$$

where μ is the air-to-plate mass ratio, defined based on the plate density (ρ), air density (ρ_∞), plate length (a), and thickness (h) as:

$$\mu = \frac{\rho_\infty}{\rho}\frac{a}{h} \quad (29)$$

The system's governing equations are established by substituting the preceding relations into the virtual work formulation expressed in Eq. (17). This procedure yields the following matrix equation:

$$\left(\omega^2[\mathbf{M}] + \omega\sqrt{\frac{\lambda\mu}{M_\infty}}[\mathbf{C_a}] + [\mathbf{K} + \lambda\mathbf{K_a}]\right)\{q\} = \{0\} \quad (30)$$

where **K** and **M** are the structural stiffness and mass matrices, respectively, and $\mathbf{K_a}$ and $\mathbf{C_a}$ denote the aerodynamic stiffness and damping matrices. To analyze the free vibration characteristics, the aerodynamic terms are omitted. Setting $\lambda = 0$ in Eq. (30) eliminates the aerodynamic pressure effects, and the governing equation takes the form of a standard eigenvalue problem:

$$(\mathbf{K} - \omega_n^2\,\mathbf{M})\,\boldsymbol{q} = \mathbf{0} \quad (31)$$

The resulting stiffness (**K**) and mass (**M**) matrices, derived from the layerwise isogeometric formulation with 7 independent degrees of freedom, are expressed as follows [31]:

$$\mathbf{K} = \int_\Omega \left\langle \sum_{k=1}^{3} \left(\begin{bmatrix} \mathbf{B}^{mb(k)} \\ \mathbf{B}^{b(k)} \\ \mathbf{B}^{s(k)} \end{bmatrix}^T \begin{bmatrix} \mathbf{A}^{(k)} & \mathbf{B}^{(k)} & \mathbf{0}_{3\times2} \\ \mathbf{B}^{(k)} & \mathbf{D}^{(k)} & \mathbf{0}_{3\times2} \\ \mathbf{0}_{2\times3} & \mathbf{0}_{2\times3} & \mathbf{E}^{(k)} \end{bmatrix} \begin{bmatrix} \mathbf{B}^{mb(k)} \\ \mathbf{B}^{b(k)} \\ \mathbf{B}^{s(k)} \end{bmatrix} \right) \right\rangle d\Omega$$

$$\mathbf{M} = \int_\Omega \left\langle \sum_{k=1}^{3} \rho^{(k)} \left(\begin{bmatrix} \mathbf{N}_1^{(k)} \\ \mathbf{N}_2^{(k)} \end{bmatrix}^T \begin{bmatrix} I_0^{(k)} & I_1^{(k)} \\ I_1^{(k)} & I_2^{(k)} \end{bmatrix} \begin{bmatrix} \mathbf{N}_1^{(k)} \\ \mathbf{N}_2^{(k)} \end{bmatrix} \right) \right\rangle d\Omega \quad (32)$$

in which $\rho^{(k)}$ is the density of the k^{th} layer, and

$$\mathbf{N}_1^{(1)} = \begin{bmatrix} 0 & \frac{-h_1}{2}R_I & 0 & \frac{-h_2}{2}R_I & 0 & 0 & 0 \\ 0 & 0 & \frac{-h_1}{2}R_I & 0 & \frac{-h_2}{2}R_I & 0 & 0 \\ R_I & 0 & 0 & 0 & 0 & 0 & 0 \end{bmatrix} \quad (33)$$

$$\mathbf{N}_2^{(1)} = \begin{bmatrix} 0 & R_I & 0 & 0 & 0 & 0 & 0 \\ 0 & 0 & R_I & 0 & 0 & 0 & 0 \\ 0 & 0 & 0 & 0 & 0 & 0 & 0 \end{bmatrix}$$

The components of the **N** matrix for the second and third layers can be derived in a similar manner. According to the linear piston theory, aerodynamic pressure is a function of the transverse displacement (w) only. Therefore, the corresponding stiffness ($\mathbf{K_a}$) and damping ($\mathbf{C_a}$) matrices are defined only in terms of the w degrees of freedom as follows:

$$\mathbf{K_a} = \int_\Omega \mathbf{B}_w \mathbf{B}_a^T\, d\Omega\ ,\ \mathbf{C_a} = \int_\Omega \mathbf{B}_w \mathbf{B}_w^T\, d\Omega \quad (34)$$

in which

$$[\mathbf{B}_w] = [R_I\ 0\ 0\ 0\ 0\ 0\ 0]^T$$
$$[\mathbf{B}_a] = [R_{I,x}\cos\Lambda + R_{I,y}\sin\Lambda\ \ 0\ 0\ 0\ 0\ 0\ 0] \quad (35)$$

Finally, the critical flutter pressure (λ_{cr}) can be determined from the eigenvalue problem in the state-space form derived from Eq. (30).

6. NUMERICAL RESULTS

This section presents numerical results to validate the proposed formulation for the free

vibration and panel flutter analysis of VSCL composite plates. Following the validation, a broad parametric study is conducted to examine the impact of key design parameters on the dynamic characteristics and aeroelastic stability boundaries. These parameters include layup configuration, degree of fiber curvature, aspect ratio, boundary conditions, and flow yaw angle in the supersonic regime. The findings of these investigations are discussed in detail in the subsequent subsections.

In general, four types of symmetric layup configurations are typically employed for VSCL plates, as follows:

- *VSC 1*: [<0, 45>/<-45, -60>/<0, 45>]
- *VSC 2*: [<30, 0>/<45, 90>/<30, 0>]
- *VSC 3*: [<90, 45>/<60, 30>/<90, 45>]
- *VSC 4*: [±<T_0, T_1>]□

The material properties employed in the free vibration analysis are:

$$E_1 = 173\ GPA\ , E_2 = 7.2\ GPA\ , \upsilon_{12} = 0.29,$$
$$G_{12} = G_{13} = G_{23} = 3.76\ GPA,$$
$$\rho = 1540\ kg/m^3$$

and for the flutter analysis, are defined as [18]:

$$E_1/E_2 = 10, G_{12}/E_2 = G_{13}/E_2 = G_{23}/E_2 = 0.33$$
$$\upsilon_{12} = 0.3, \rho = 1$$

The analysis considers two types of boundaries conditions: fully clamped (CCCC) and simply supported (SSSS). For the clamped case, all seven degrees of freedom are constrained along each edge of the plate. For the simply supported condition, however, only the following degrees of freedom are set to zero:

- For edges parallel to the x-axis:

$$u_0 = v_0 = w_0 = \psi_y^{(k)} = 0$$

- For edges parallel to the y-axis:

$$u_0 = v_0 = w_0 = \psi_x^{(k)} = 0$$

The isogeometric analysis utilizes cubic NURBS basis functions with a four-point Gauss quadrature for numerical integration. The selection of these numerical parameters follows established IGA practice. Cubic (p=3) NURBS provide the C^2-continuity ideal for accurately capturing plate bending curvature. The corresponding four-point (p+1) Gauss quadrature rule ensures full, stable, and accurate integration of the element matrices.

Table 1. Convergence study of a simply supported VSCL plate with h/b = 0.01.

No. of El.	Method	Layup		
		VSC 1	VSC 2	VSC 3
7x7	LWT IGA	57.23	49.24	52.98
9x9		57.05	49.17	52.61
11x11		56.94	49.15	52.44
13x13		56.87	49.14	52.35
15x15		56.82	49.14	52.28
	TSDT [4]	57.06	49.15	52.47
	UEM 1 [7]	56.78	49.14	52.26
	UEM 3 [7]	56.74	49.13	52.24

6.1 Free Vibration Analysis

This section begins with a convergence study of the free vibration response for a three-layer, variable-stiffness composite laminate. Subsequently, after the validation and comparison of the obtained results with those available in the literature, the effects of fiber path variations and boundary conditions on the vibrational behavior of a symmetric, four-layer VSCL plate are studied.

To investigate convergence, the fundamental frequencies (in Hz) for a simply supported, symmetric VSCL plate with three layup configurations (VSC 1 to VSC 3) are presented in Table 1. As observed, for a square plate with a thickness-to-width ratio (h/b) of 0.01, the results demonstrate that a 15×15 element mesh provides excellent convergence. This highlights the high computational efficiency of the IGA approach, as a recent layerwise study using the conventional Finite Element Method required a much finer 30×30 mesh to achieve convergence [7]. Therefore, a 15×15 mesh is adopted for all subsequent computations.

Table 2. The first four natural frequencies of a VSCL plates for different thickness ratio and BC's.

Layup	*h/b*	Method	BC's : SSSS				BC's : CCCC			
			Mode				Mode			
			1	2	3	4	1	2	3	4
VSC 1	0.01	LWT (FSDT IGA)	56.82	93.62	152.67	170.87	92.27	130.81	195.25	238.07
		LWT (FSDT) [7]	56.78	93.56	152.57	170.80	92.25	130.76	195.06	237.92
		LWT (TSDT) [7]	56.74	93.49	152.46	170.66	92.18	130.67	194.92	237.54
	0.1	LWT (FSDT IGA)	468.86	746.41	1134.38	1164.16	618.46	910.21	1238.81	1331.48
		LWT (FSDT) [7]	468.66	746.23	1134.28	1164.10	618.41	910.17	1238.78	1331.47
		LWT (TSDT) [7]	461.60	734.93	1107.02	1146.61	605.49	893.80	1206.46	1307.55
VSC 2	0.01	LWT (FSDT IGA)	49.14	80.18	134.61	180.08	106.24	137.42	196.76	271.38
		LWT (FSDT) [7]	49.14	80.18	134.54	180.05	106.22	137.36	196.51	270.88
		LWT (TSDT) [7]	49.13	80.16	134.51	179.94	106.14	137.26	196.36	270.53
	0.1	LWT (FSDT IGA)	421.30	677.58	1074.64	1159.87	663.55	908.67	1299.42	1303.67
		LWT (FSDT) [7]	421.25	677.58	1074.66	1159.87	663.53	908.69	1299.45	1303.73
		LWT (TSDT) [7]	416.49	670.58	1061.40	1130.81	648.44	892.51	1268.38	1277.49
VSC 3	0.01	LWT (FSDT IGA)	52.28	85.38	140.42	172.92	113.13	145.22	212.68	269.31
		LWT (FSDT) [7]	52.26	58.33	140.26	172.75	113.08	145.09	212.11	268.64
		LWT (TSDT) [7]	52.24	85.30	140.21	172.63	112.98	144.97	211.91	268.22
	0.1	LWT (FSDT IGA)	440.05	704.20	1109.87	1146.49	686.35	920.17	1299.52	1312.38
		LWT (FSDT) [7]	439.74	703.97	1109.85	1146.25	686.34	920.18	1299.48	1312.40
		LWT (TSDT) [7]	434.30	695.78	1095.57	1118.98	670.22	902.88	1263.80	1288.50

To confirm the accuracy of the free vibration analysis, the first four natural frequencies of a square plate are shown in Table 2 for three different layup configurations (VSC 1, VSC 2, and VSC 3) under both simply-supported and clamped boundary conditions. The results are given for thickness-to-width ratios (*h/b*) of 0.1 and 0.01. These findings are compared with data from layerwise models used as User Elements (UEL) in Abaqus, which utilize first- and third-order shear deformation theories (UEM and UEM3 models) applied to each individual layer [7]. The current formulation shows remarkable consistency, especially with the UEM1 model.

Having established the convergence and validity of the model, the analysis is extended to the free vibration of four-layer composite plates with curvilinear fibers. The VSC 4 layup scheme is considered for a plate with *h/b*=0.1 under both fully clamped and simply-supported conditions. Tables 3 and 4 present the first five natural frequencies for the $[\pm\langle\theta, 45\rangle]_S$ and $[\pm\langle 45, \theta\rangle]_S$ configurations, respectively, where the angle θ is varied from 0° to 90°.

Table 3. The first five natural frequencies for a $[\pm\langle\theta, 45\rangle]_S$ laminate ($h/b = 0.1$).

BC's	θ	Mode				
		1	2	3	4	5
SSSS	0	486.4	752.9	1131.9	1149.7	1381.9
	15	497.7	808.7	1129.1	1218.8	1433.2
	30	505.5	875.7	1107.9	1324.1	1521.5
	45	506.0	916.7	1100.2	1365.9	1620.5
	60	498.3	885.0	1129.3	1332.5	1546.0
	75	484.5	809.5	1162.0	1249.4	1444.8
	90	471.7	739.2	1170.9	1180.1	1369.2
CCCC	0	623.1	894.1	1250.2	1294.2	1487.0
	15	634.6	946.1	1237.7	1362.8	1541.2
	30	651.3	1022.5	1227.0	1454.0	1636.6
	45	669.3	1077.7	1227.1	1496.0	1728.7
	60	681.9	1057.5	1257.1	1478.2	1658.2
	75	690.2	994.7	1292.0	1419.2	1560.3
	90	695.1	946.9	1315.0	1369.2	1490.5

Table 4. The first five natural frequencies for a $[\pm\langle 45, \theta\rangle]_S$ laminate ($h/b = 0.1$).

BC's	θ	Mode				
		1	2	3	4	5
SSSS	0	0	443.4	792.1	1148.6	1235.0
	15	15	467.8	851.3	1130.8	1293.9
	30	30	493.3	901.2	1114.7	1345.0
	45	45	506.0	916.7	1100.2	1365.9
	60	60	498.8	884.2	1091.1	1336.7
	75	75	467.8	803.2	1082.1	1250.0
	90	90	431.2	716.6	1077.4	1159.2
CCCC	0	0	686.6	1013.5	1296.6	1446.0
	15	15	689.0	1047.1	1275.5	1473.2
	30	30	682.6	1075.8	1249.3	1493.9
	45	45	669.3	1077.7	1227.1	1496.0
	60	60	652.1	1035.9	1218.5	1470.9
	75	75	637.8	974.9	1217.4	1421.8
	90	90	629.7	932.0	1218.0	1381.3

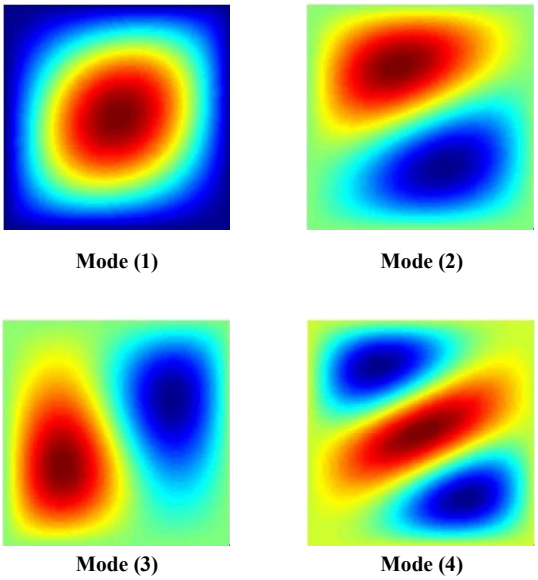

Fig. 3. The first four mode shapes for a clamped [±<30, 45>]□ laminate with $h/b = 0.1$.

6.2 Flutter Analysis

To validate the panel flutter analysis, the critical dynamic pressure for a four-layer, variable-stiffness composite laminate is first calculated and compared with established results from the literature. Following this validation, a parametric study is completed to examine the effect of fiber curvature (via T_0 and T_1 variations), the supersonic flow yaw angle, and the boundary conditions on the aeroelastic stability. The aerodynamic damping parameter in the free stream (μ/M_∞) is set to 0.01, while h/b is equal to 0.01.

A comparative analysis is conducted to validate the present Layerwise Theory (LWT) against the first- and higher-order shear deformation presented by Khalafi and Fazilati [18] and Sharma et al. [34], respectively. The case study involves a simply-supported square plate (h/b = 0.01) with a [±<20, 40>]$_S$ layup (VSC 4) under zero yaw angle flow. The relationship between the non-dimensional aerodynamic pressure and the eigen frequency is illustrated in Fig. 4. The critical flutter point is identified as the condition where two frequency modes approach and coalesce, leading to structural instability. As depicted in Fig. 4, there is excellent agreement between the results of the present model and the cited references. However, a slight discrepancy is observed, with the LWT model predicting a slightly lower critical flutter speed and frequency than the other two ESL theories.

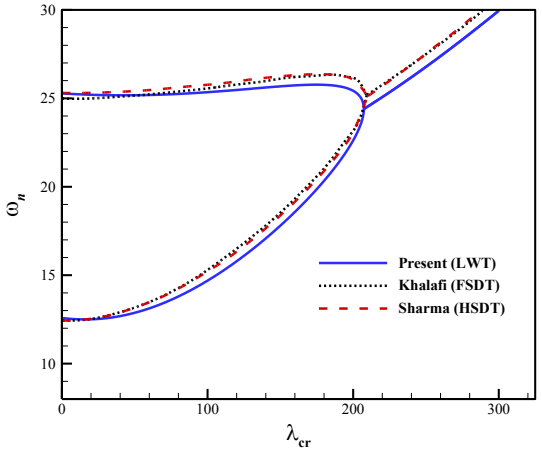

Fig. 4. Frequency coalescence of simply-supported 4-layer VSCL plate with a [±<20, 40>]$_S$ layup.

Table 5. The critical flutter pressure for a simply-supported [±<40, 60>]$_S$ laminate for different yaw angles.

No. of EL	Method	Yaw Angle (Λ)			
		0°	30°	60°	90°
7×7	LWT (IGA)	154.90	224.70	253.88	170.86
9×9		155.56	225.92	256.05	172.10
11×11		155.86	226.42	256.26	172.32
13×13		155.94	226.49	256.27	172.34
15×15		155.96	226.50	256.28	172.36
17×17		155.96	226.50	256.28	172.36
	FSDT IGA [18]	156.6	227.8	256.6	172.9

To complement the free vibration analysis, a convergence study was conducted specifically for the critical flutter pressure, as detailed in Table 5. The analysis for a [±<40, 60>]$_S$ VSCL plate under various yaw angles demonstrates excellent convergence. The results from the 15×15 mesh are nearly identical to those from the finer 17×17 mesh, indicating that the solution has stabilized. Based on these findings, and in agreement with the vibration study, a 15×15 element mesh is selected for all subsequent flutter analyses.

The influence of fiber curvature (T_0 and T_1) and flow yaw angle on the critical aerodynamic pressure (λ) is depicted in Figs. 5 and 6. These results correspond to a simply supported VSC 4 composite plate with $h/b = 0.01$ for two different layup schemes [±<T_0, θ>]$_S$ and [±<θ, T_1>]$_S$.

Figure 5(a) shows the variation of the critical flutter pressure as the edge angle (T_1) is swept from 0° to 90°, while the center angle (T_0) is held constant at 20°, 40°, 60°, and 80°. As shown, the critical flutter speed consistently decreases with increasing T_1. Moreover, for any given T_1, a lower value of T_0 yields a higher flutter speed, indicating that for this layup, lower fiber angles at the plate's center result in more favorable aeroelastic stiffness. Conversely, Fig. 5(b) illustrates the effect of varying the center control angle (T_0) from 0° to 90°, while keeping the edge angle (T_1) constant at 20°, 40°, 60°, and 80°. The trend observed is consistent with the previous case: as T_0 increases, there is a steady decrease in the critical flutter speed. This finding suggests that for the given layup, any increase in fiber curvature, whether originating from the center or the edges, degrades the overall aeroelastic stiffness of the plate, thereby reducing its resistance to flutter.

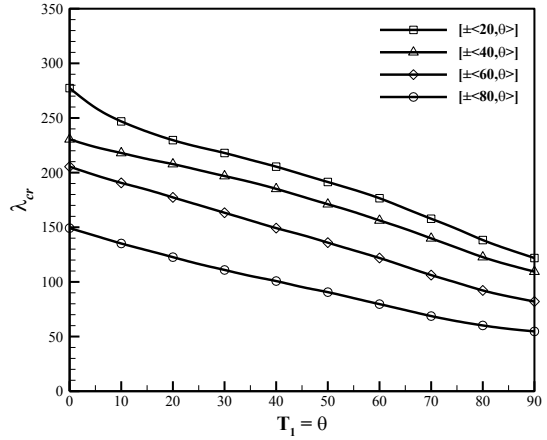

(a) [±<T_0, θ >]$_S$

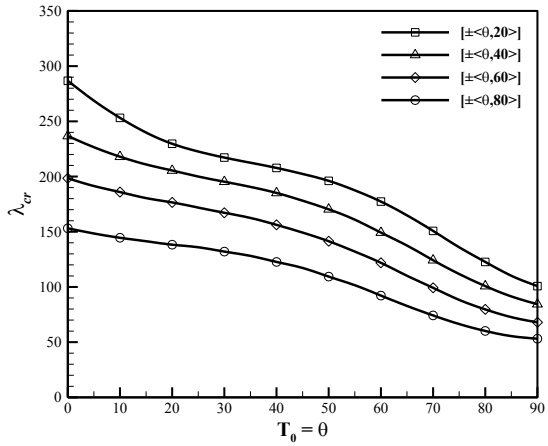

(b) [±<θ.,T_1>]$_S$

Fig. 5. Effect of fiber curvature on the flutter boundary of a four-layer VSCL plate with $\Lambda = 0$ for **(a)** [±<T_0, θ>]$_S$ and **(b)** [±<θ, T_1>]$_S$ layups.

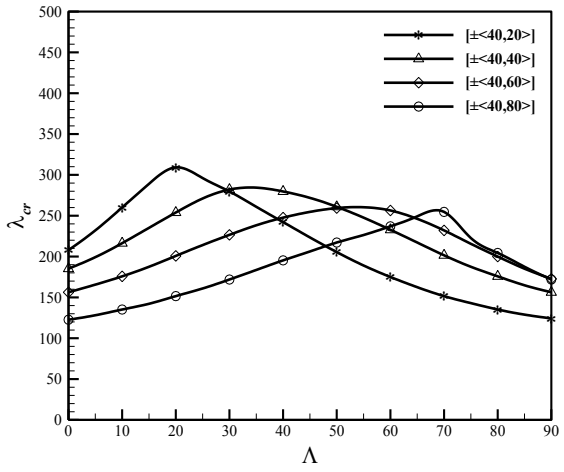

(a) [±<40, T_1>]$_S$

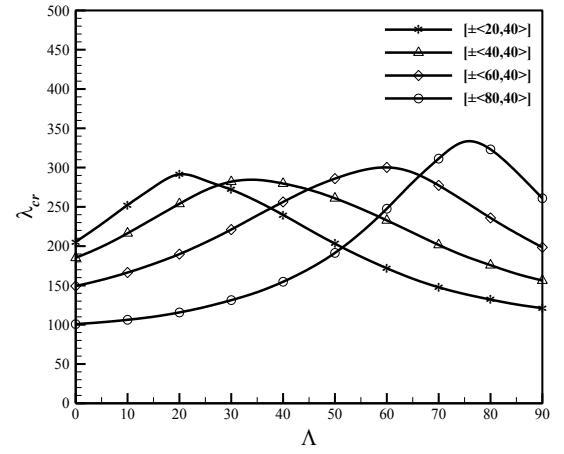

(b) [±<T_0, 40>]$_S$

Fig. 6. Effect of flow yaw angle on the flutter boundary of a four-layer VSCL plate with **(a)** [±<T_0, 40>]$_S$ and **(b)** [±<40, T_1>]$_S$ layups.

Next, the effect of the supersonic yaw angle on the critical flutter pressure is presented in Fig. 6. Figure 6(a) shows this relationship for the [±<40, T_1>]$_S$ layup, where the control angle T_1 is set to 20°, 40°, 60°, and 80°. As illustrated in Fig. 6(a), the layup with T_1 = 20° configuration reaches its maximum aeroelastic stability at low yaw angles. In contrast, the layup with T_1 = 80° configuration achieves its peak flutter performance at a significantly higher yaw angle, near 70°. The complementary case is shown in Fig. 6(b), which analyzes the [±<T_0, 40>]$_S$ configuration. Here, the edge angle (T_0) is the variable parameter while the center angle is fixed at 40°. It is again evident from the graph that adjusting T_0 allows the yaw angle corresponding to the maximum flutter speed to be effectively controlled.

Finally, to investigate the effect of boundary conditions on the aeroelastic stability of variable-stiffness composite laminates (VSCLs), the critical aerodynamic pressure is plotted as a function of the yaw angle in Fig. 7. The analysis is conducted for a plate with a $[\pm\langle 40, 60\rangle]_S$ layup with h/b=0.01. Both simply-supported (SSSS) and clamped (CCCC) cases are considered and compared against reference FSDT data from Khalafi and Fazilati [18]. A minor discrepancy is noted for this configuration, with the present LWT predicting a slightly lower flutter speed for the clamped case compared to the ESL theory. The findings show that boundary conditions play an important role in determining the flutter boundary. As expected, when the bending stiffness increases with a clamped condition, the flutter speed becomes higher than in the simply-supported case.

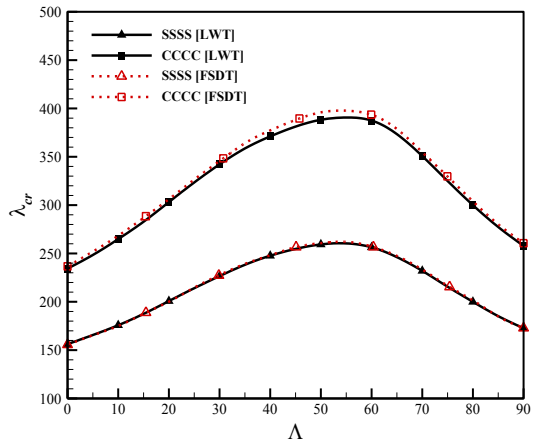

Fig. 7. Effect of BC's on the flutter boundary of a four-layer VSCL plate with $[\pm\langle 40, 60\rangle]_S$ for different flow yaw angles.

7. CONCLUSION

The IGA framework was developed for the free vibration and panel flutter analysis of variable-stiffness composite plates. This approach utilizes the NURBS functions to serve simultaneously as the geometric description and the basis for the field approximation. The governing equations were established using Hamilton's principle, incorporating Ferreira's layerwise model with FSDT theory for each layer and first-order piston theory for modeling aerodynamic forces. After establishing the model's accuracy through convergence and validation studies on three- and four-layer VSCL plates, a parametric investigation was conducted. The role of boundary conditions, flow yaw angle, fiber curvature, and layup schemes on the dynamic and aeroelastic behavior of laminates were examined. The key findings from this research are:

- Within the isogeometric framework, the results from the Ferreira layerwise model demonstrated excellent agreement with established layerwise models in the literature.
- For the free vibration analysis of moderately thick plates, the layerwise model was found to yield more accurate results compared to ESL theories.
- The study demonstrated that employing curvilinear fibers in variable-stiffness laminates offers a significant advantage in both vibrational and aeroelastic performance over conventional straight-fiber composite plates.

As expected, the eigen frequencies and the aeroelastic instability boundary of the VSCL plate were consistently higher for clamped boundary conditions than for simply supported conditions, which is attributed to the increased structural stiffness inherent to the clamped configuration.

In summary, the developed isogeometric layerwise framework serves as a robust and accurate computational tool for the analysis and design of advanced composite structures, offering a reliable path for optimizing their vibrational and aeroelastic performance through tailored fiber placement.

CONFLICTS OF INTEREST

The authors declare that they have no conflict of interest.

REFERENCES

[1] M. W. Hyer and R. F. Charette, "Use of curvilinear fiber format in composite structure design," *AIAA Journal*, vol. 29, no. 6, pp. 1011–1015, 1991, https://doi.org/10.2514/3.10697.

[2] S. Nagendra, S. Kodiyalam, J. Davis, and V. Parthasarathy, "Optimization of tow fiber paths for composite design," in *36th Structures, Structural Dynamics and Materials Conference*, New Orleans, LA, USA, 1995, paper 1275. https://doi.org/10.2514/6.1995-1275.

[3] M. M. Abdalla, S. Setoodeh, and Z. Gürdal, "Design of variable stiffness composite panels for maximum fundamental frequency using lamination parameters," *Composite Structures*, vol. 81, no. 2, pp. 283–291, 2007, https://doi.org/10.1016/j.compstruct.2006.08.018.

[4] H. Akhavan and P. Ribeiro, "Natural modes of vibration of variable stiffness composite laminates with curvilinear fibers," *Composite Structures*, vol. 93, no. 11, pp. 3040–3047, 2011, https://doi.org/10.1016/j.compstruct.2011.04.027.

[5] S. Yazdani and P. Ribeiro, "A layerwise p-version finite element formulation for free vibration analysis of thick composite laminates with curvilinear fibres," *Composite Structures*, vol. 120, pp. 531–542, 2015, https://doi.org/10.1016/j.compstruct.2014.10.030.

[6] M. Hachemi, A. Guenanou, R. Chebout, and K. Bachari, "Mechanical behaviors of variable stiffness composite laminated sandwich plates using layer-wise model," *Journal of the Brazilian Society of Mechanical Sciences and Engineering*, vol. 45, no. 2, 2023, Art. no. 77, https://doi.org/10.1007/s40430-022-03949-2.

[7] J. A. Moreira, F. Moleiro, A. L. Araújo, and A. Pagani, "Assessment of layerwise user-elements in Abaqus for static and free vibration analysis of variable stiffness composite laminates," *Composite Structures*, vol. 303, 2023, Art. no. 116291, https://doi.org/10.1016/j.compstruct.2022.116291.

[8] T. J. R. Hughes, J. A. Cottrell, and Y. Bazilevs, "Isogeometric analysis: CAD, finite elements, NURBS, exact geometry and mesh refinement," *Computer Methods in Applied Mechanics and Engineering*, vol. 194, no. 39–41, pp. 4135–4195, 2005, https://doi.org/10.1016/j.cma.2004.10.008.

[9] S. Shojaee, N. Valizadeh, E. Izadpanah, T. Bui, and T. V. Vu, "Free vibration and buckling analysis of laminated composite plates using the NURBS-based isogeometric finite element method," *Composite Structures*, vol. 94, no. 5, pp. 1677–1693, 2012, https://doi.org/10.1016/j.compstruct.2012.01.012.

[10] C. H. Thai, A. J. M. Ferreira, E. Carrera, and H. Nguyen Xuan, "Isogeometric analysis of laminated composite and sandwich plates using a layerwise deformation theory," *Composite Structures*, vol. 104, pp. 196–214, 2013, https://doi.org/10.1016/j.compstruct.2013.04.002.

[11] Y. Guo, A. P. Nagy, and Z. Gürdal, "A layerwise theory for laminated composites in the framework of isogeometric analysis," *Composite Structures*, vol. 107, pp. 447–457, 2014, https://doi.org/10.1016/j.compstruct.2013.08.016.

[12] N. Liu and A. E. Jeffers, "Isogeometric analysis of laminated composite and functionally graded sandwich plates based on a layerwise displacement theory," *Composite Structures*, vol. 176, pp. 143–153, 2017, https://doi.org/10.1016/j.compstruct.2017.05.037.

[13] J. Fazilati and V. Khalafi, "Panel flutter analysis of perforated plate repaired by VSCL bonded patch using the multi-patch IGA approach," *Thin-walled structures*, vol. 169, 2021, Art. no. 108465, https://doi.org/10.1016/j.tws.2021.108465.

[14] K. A. Hasim and A. Kefal, "Isogeometric static analysis of laminated plates with curvilinear fibers based on refined zigzag theory," *Composite Structures*, vol. 256, 2021, Art. no. 113097, https://doi.org/10.1016/j.compstruct.2020.113097.

[15] K. A. Hasim and A. Kefal, "A novel isogeometric layerwise element for piezoelectric analysis of laminated plates with straight/curvilinear fibers," *Computer Methods in Applied Mechanics and Engineering*, vol. 399, 2022, Art. no. 115440, https://doi.org/10.1016/j.cma.2022.115440.

[16] K. A. Hasim and A. Kefal, "Free and forced vibration analysis of piezolaminated plates via an isogeometric layerwise finite element," *Mechanics of Advanced Materials and Structures*, vol. 32, no. 17, pp. 4146-4161, 2024, https://doi.org/10.1080/15376494.2024.2400716.

[17] O. A. Stodieck, J. E. Cooper, P. M. Weaver, and P. Kealy, "Optimization of tow-steered composite wing laminates for aeroelastic tailoring," *AIAA Journal*, vol. 53, no. 8, pp. 2203-2215, 2015, https://doi.org/10.2514/1.J053599.

[18] V. Khalafi and J. Fazilati, "Supersonic panel flutter of variable stiffness composite laminated skew panels subjected to yawed flow by using NURBS-based isogeometric approach," *Journal of Fluids and Structures*, vol. 82, pp. 198-214, 2018, https://doi.org/10.1016/j.jfluidstructs.2018.07.002.

[19] J. Fazilati and V. Khalafi, "Aeroelastic panel flutter optimization of tow-steered variable stiffness composite laminated plates using isogeometric analysis," *Journal of Reinforced Plastics and Composites*, vol. 38, no. 19-20, pp. 885-895, 2019, https://doi.org/10.1177/0731684419854800.

[20] J. Fazilati, "Panel flutter of curvilinear composite laminated plates in the presence of delamination," *Journal of Composite Materials*, vol. 52, no. 20, pp. 2789-2801, 2018, https://doi.org/10.1177/0021998318754641.

[21] H. Akhavan and P. Ribeiro, "Aeroelasticity of composite plates with curvilinear fibres in supersonic flow," *Composite Structures*, vol. 194, pp. 335-344, 2018, https://doi.org/10.1016/j.compstruct.2018.03.101.

[22] M. Rahmanian, T. Farsadi, and H. Kurtaran, "Nonlinear flutter of tapered and skewed cantilevered plates with curvilinear fiber paths," *Journal of Sound and Vibration*, vol. 500, 2021, Art. no. 116021, https://doi.org/10.1016/j.jsv.2021.116021.

[23] M. M. Navardi, H. Shahverdi, and V. Khalafi, "Aeroelastic tailoring of variable stiffness composite laminated quadrilateral and circular plates in supersonic flow using isogeometric approach," *International Journal of Applied*

Mechanics, vol. 15, no. 1, 2023, Art. no. 2250091, https://doi.org/10.1142/S1758825122500910.

[24] M. M. Navardi, H. Shahverdi, and V. Khalafi, "Isogemetric aeroelastic analysis of composite cylindrical panels with curvilinear fibers," *Steel and Composite Structures*, vol. 52, no. 5, pp. 515-524, 2024, https://doi.org/10.12989/scs.2024.52.5.515.

[25] P. Hao, J. Duan, Y. Liu, Y. Gao, Y. Yue, and W. Wang, "Aerothermoelastic behaviors of curvilinear fiber composite panels based on the refined zig-zag theory," *Archive of Applied Mechanics*, vol. 94, pp. 3803-3823, 2024, https://doi.org/10.1007/s00419-024-02696-1.

[26] J. Fazilati, V. Khalafi, and M. Jalalvand, "Panel flutter analysis of nano-hybrid laminated composite quadrilateral plates presuming curvilinear fibers," *Mechanics Based Design of Structures and Machines*, vol. 52, no. 10, pp. 8198-8215, 2024, https://doi.org/10.1080/15397734.2024.2316870.

[27] J. A. Moreira, F. Moleiro, A. Araújo, and A. Pagani, "Equivalent single layer and layerwise models for flutter and buckling analysis of supersonic variable stiffness laminated composite plates," *Thin-Walled Structures*, vol. 191, 2023, Art. no. 111012, https://doi.org/10.1016/j.tws.2023.111012.

[28] J. A. Moreira, F. Moleiro, A. L. Araújo, and A. Pagani, "Layerwise models for supersonic flutter analysis of viscoelastic sandwich panels with curvilinear fibre composite skins," *Journal of Sound and Vibration*, vol. 572, 2024, Art. no. 118182, https://doi.org/10.1016/j.jsv.2023.118182.

[29] J. A. Moreira, F. Moleiro, A. L. Araújo, and A. Pagani, "Aero-thermo-elastic stability analysis of supersonic variable stiffness sandwich panels using refined layerwise models," *Composite Structures*, vol. 357, 2025, Art. no. 118920, https://doi.org/10.1016/j.compstruct.2025.118920.

[30] J. A. Moreira, F. Moleiro, A. L. Araújo, and A. Pagani, "Active aero-visco-elastic flutter control and layerwise modelling of supersonic smart sandwich panels with variable stiffness composites," *Aerospace Science and Technology*, vol. 157, 2025, Art. no. 109847, https://doi.org/10.1016/j.ast.2024.109847.

[31] M. Dabouee, V. Khalafi, and H. Zarei, "Layerwise isogeometric analysis for free vibrations of VSCL plates with arbitrary shapes," *International Journal of Applied Mechanics*, vol. 17, no. 10, 2025, Art. no. 2550091, https://doi.org/10.1142/S1758825125500917.

[32] J. Fazilati and V. Khalafi, "Effects of embedded perforation geometry on the free vibration of tow-steered variable stiffness composite laminated panels," *Thin-Walled Structures*, vol. 144, 2019, Art. no. 106287, https://doi.org/10.1016/j.tws.2019.106287.

[33] J. W. Sawyer, "Flutter and buckling of general laminated plates," *Journal of Aircraft*, vol. 14, no. 4, pp. 387–393, 1977, https://doi.org/10.2514/3.58789.

[34] N. Sharma, S. Mohapatra, E. K. Kumar, and S. K. Panda, "Numerical aeroelastic flutter prediction of variable stiffness laminated panels with curvilinear fiber in supersonic flow," *Structures*, vol. 57, 2023, Art. no. 105198, https://doi.org/10.1016/j.istruc.2023.105198.